Advances in Science and Technology Research Journal, 2025, 19(12), 341–360 https://doi.org/10.12913/22998624/210152 ISSN 2299-8624, License CC-BY 4.0

Multi-objective optimization of thin-walled hybrid frusta acting as collision energy absorbers

Karol Szklarek^{1*}, Maria Kotełko²

- ¹ Faculty of Mechanical Engineering, Lublin University of Technology, Nadbystrzycka 36, 20-618 Lublin, Poland
- ² Department of Strength of Materials, Łodź University of Technology, Łódź, Poland
- * Corresponding author's e-mail: k.szklarek@pollub.pl

ABSTRACT

This paper presents a multi-objective optimization study of thin-walled prismatic frusta (truncated pyramids) designed as crash energy absorbers. The research involved over 130 geometric variants, including both hollow and EPP foam-filled configurations, analyzed using finite element simulations and validated through experimental impact tests. A data-driven optimization algorithm, based on artificial neural networks (ANNs), was developed to enable fast prediction of crashworthiness parameters such as absorbed energy, peak crushing force, and total efficiency. To demonstrate practical applicability, the algorithm was used to optimize structural elements of a homologation vehicle frame in accordance with Regulation No. 29 of the UN ECE, achieving targeted energy absorption while respecting design constraints. Increasing the apex angle α reduces peak crushing force (PCF) in both hollow and filled frusta. Foam filling increases PCF, but its effect on crush load efficiency (CLE) varies with α . Filling improves total efficiency (TE) in hollow frusta significantly, while the effect is geometry-dependent in filled variants. The ANN-based tool reduces design iteration time and supports early-stage decisions in the development of crashworthy structures. These results contribute to the advancement of lightweight, energy-efficient safety components in vehicle design.

Keywords: collision energy absorption, thin-walled absorbers, optimization, artificial neuron networks

INTRODUCTION

During the design of a vehicle, aircraft, or marine vessel, there is a need to develop elements responsible for energy absorption, which in turn ensures the safety of participants in hazardous events. One of the most important safety features in a vehicle is an effective system (structure) that is capable of absorbing collision energy, thereby reducing injuries to those involved in the collision. Related safety considerations in structural engineering include fire-induced thermal exposure of steel components and their thermal design, which critically affects residual load-carrying capacity and the time available for safe evacuation [1]. Currently, there is pressure to design lightweight, compact vehicles, which allows for a reduction in fuel consumption and emissions. These requirements necessitate the use of lightweight, economical, and

easy-to-manufacture and assemble energy-absorbing structures – energy absorbers.

Received: 2025.08.06

Accepted: 2025.10.01

Published: 2025.11.01

Such a structural member termed energy absorber converts entirely or partially a kinetic energy into another form of energy. One of the possible solutions is the conversion of the kinetic energy of impact into the energy of plastic deformation of a thin-walled metallic or hybrid (metallic-foam filled) structural member There are numerous types of energy absorbers of that kind that are cited in the literature [2]. Beyond axial crushing, the dynamic stability of thin-walled shell-type members under transient loading has also been extensively investigated, including formulations with ductile damage evolution based on Lemaitre's model, highlighting how material softening and damage can shift critical thresholds[3]. Thin-walled members used in the design of energy absorbers have been of interest to researchers since the 1960s. The most popular shapes of energy absorbing structures (Figure 1) are: cylindrical, rectangular, or polygonal tubes subjected to axial and lateral (radial) compression, compressed truncated cones (frustums) and rods, compressed honeycomb structures, compressed multilayer structures, compressed omega (top hat) structures, and crushed corrugated or graduated tubes [4, 5].

One of the ways to increase energy absorption capacity while maintaining the lowest possible mass of energy absorbers is to fill them with a lightweight material that can deform significantly under nearly constant crushing load. Such materials include, among others, fiber-reinforced polyamide, cork, wood, polyurethane foam, nano polyurethane foam, and metal foam. Among these, both polymer and metal foams are gaining increased interest. The behavior of the foam depends on its cellular microstructure, properties, and relative density of the material, as the mechanism of deformation of the foam material at the cellular level is regulated by bending and stretching of the cell walls, followed by buckling and tearing at the stage of achieving plasticity [6]. In general, the mechanical strength of the foam material increases with the increase in relative density [7].

Additionally, there is interfacial friction between the filling material and the wall of the tube. This causes the crushing force of the foam-filled tube to be higher than the sum of the crushing forces of the empty tube and the foam when they are crushed separately, i.e., a synergy phenomenon occurs [8]. Complementary to crashworthiness in axial crushing, recent studies on multicellular thin-walled tubes under torsion have applied variance-based sensitivity analysis and data-driven optimization to map how geometry and material parameters control stiffness and stress, offering transferable meta-modeling strategies for lightweight design [9].

Structural members termed "frusta" (*frustum* – from Latin: piece, bite) are used as energy absorbers due to the stable plastic behavior during axial crushing process and due to the decrease of peak crushing load in comparison with cylindrical columns or parallelepiped-shaped thin-walled columns. The possible shapes of such members are thin-walled truncated cones or prisms.

Several authors present a comparison of frustums with different cross-sectional shapes [10, 11]. Many researchers have analyzed the type of cylindrical frustum (truncated cone). The results of research on this type of structural member and various modifications are the subject of a number of works [12-49]. For frustums with rectangular or square cross-sections, the literature is more limited. One of the first works on this topic is the work of Reid [50], which compared the energy absorption capacity of metal tubes with a single inclined wall, two walls, and three walls in comparison to a tube without inclination. The studies were conducted under both quasi-static and dynamic axial loading conditions. Additionally, the issue of oblique impact response was also considered. Mamalis [51] defined the mode of deformation and axial load characteristics of cylindrical and prismatic frustums made of PVC. In the work of Mamalis [52] he examined the impact resistance of a square cross-section frustum made of glass composite. The same author, in paper [53], compared the results of experimental tests with those obtained from FEM for four variants of the frustum. A significant contribution to the study of prismatic frustums was made by Nagel and Thambiratnam. They investigated the energy absorption capacity of simple and pyramidal tubes subjected to axial impact using FEM [54]. The research took into account the number of inclined walls, the angle of inclination, the wall thickness, the impact velocity, and the duration of the impact itself. It

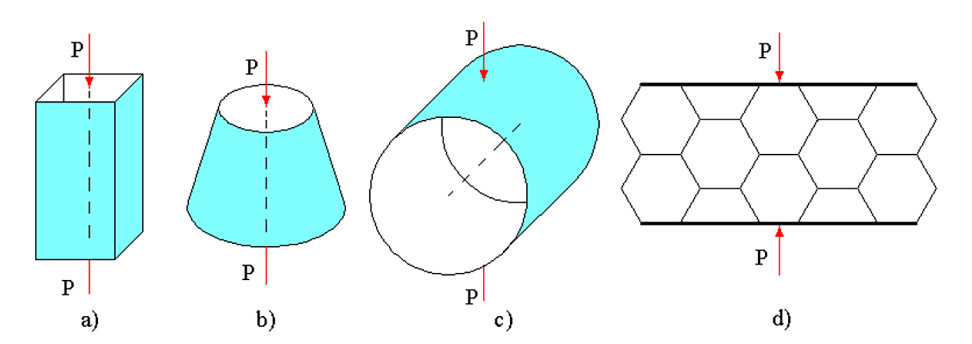


Figure 1. Energy absorber design solutions: a) rectangular tube – axial load, b) frustum, c) round tube – radial load, d) honeycomb structure

was found that frustums have a higher crushing force efficiency than straight tubes, and that impact velocity has less influence on the absorbed energy compared to straight tubes. The studies were conducted for a rectangular cross-section. In the work [55], the authors demonstrated that the energy absorption of pyramidal tubes can be controlled by their wall thickness and the apex angle. However, the studies were conducted exclusively for pyramids with two opposite inclined walls and a rectangular cross-section.

Researchers in work [56] expanded their studies on frustums with inclined 3 and 4 walls. It was assumed that the base in the narrower part is fixed. In the case of sloping walls, the crosssection of the frustum base was increased. Liu [57] conducted optimizations of a frustum with a square section using the RSM (response surface methodology). He chose the following optimization parameters: wall thickness, angle of inclination (apex angle), and, like previous researchers, the dimensions of the smaller cross-section. The optimization was done for SEA (Specific Energy) and the ratio Favg/Fmax. He assumed constant impact energy. He concluded that the optimal angle of inclination (apex angle) is equal to 5°, for the smallest cross-section area and for the largest wall thickness studied. Qi et al [58] considered a frustum with a square section during oblique impact. They related the results to simple elements and additionally in a filling version (singlecell and multi-cell). Additionally, the researchers conducted multi-objective optimization (MOD) to maximize SEA and minimize PCF strength. During the MOD optimization, they created accurate surrogate models, specifically response surface models (RS) for SEA and PCF to reduce the computational costs of finite element method simulations of collisions. Asanjarani [59] conducted similar research. Unlike his predecessor, he took into account the indentations in the walls of energy absorbers, and the optimization was for the case of an axial impact. Gan [60] studied the behavior of frustums in various configurations, calling it 'multi-frusta'. They arranged four frustums in different ways to create a single energy-absorbing structure. This way, they investigated the mutual cooperation of these systems. The research was conducted for the axial loading case. Unlike multi-cell systems, here the energy absorber consisted of several smaller ones. Additionally, a multi-objective optimization was performed. Altin [61] examined four different

types of multi-cell tubes, including frustum. For each type, he designed seven different multi-cell structures. One example of the use of a frustum shape with a square cross-section is shown by Hong [62], who employs this shape in an energy-absorbing construction used in subway cars. An interesting study regarding frustums is the research by Hong [62], who investigated one of the few triangular cross-section frustums.

As already mentioned, recent research directions on frustums mainly focus on cylindrical frustums. Patel [34] analyzed the resistance to crushing of monolithic and co-axial multilayered (two-, three-, and four-layered) tubular frustum-type structures subjected to quasi-static axial loading. The grey relational analysis (GRA) method was applied for optimization, the results of which showed that multi-layer structures reduce the peak force, and the three-layer configuration provides the best impact properties. Kathiresan [38] examined the effect of different shapes, sizes, and the number of side cutouts in various locations on the load-bearing capacity, buckling, and energy absorption characteristics (E_{obs}) of aluminum conical frustum profiles under quasi-static axial loading conditions. It has been shown that circular holes are the most advantageous. The same author in work [39] examined the impact of these circular cutouts on axial and oblique low-speed impacts. Feli [37] studied the effect of radial grooves in conical frustums using a new analytical model. He demonstrated that creating such grooves allows for greater control over the crushing process and reduces the peak force. Akhavan [40] investigated the behavior during the crushing of interlocking steel frustums with different arrangements and cross-sections, both in experimental and numerical analysis, under quasi-static axial loading. Tuzgel [41], inspired by biology (buds), studied the impact resistance of sandwich two-layer structures, in which cylindrical frusta with modified fillings were used for infill. He demonstrated that such a structure has a higher capacity to absorb energy than its components. Chen [42] created composite single-layer, double-layer, and foam-filled conical CFRC tubes. He discussed and compared the crushing modes with simple tubes, showing that compared to simple circular tubes, conical tubes have more progressive folding and significantly better crush force efficiency (CFE).

The detailed description of the research on frustums presented above shows a prevailing

analysis of cylindrical frustums. The studies concerning prismatic frustums are less extensive. There is a lack of detailed parametric analysis. The multi-criteria optimization methods RMS involved optimizing indicators of energy absorption such as specific energy absorption (SEA), the ratio of average crushing force to maximum crushing force F_{avo}/F_{max} , and the first peak value of the crushing force. Researchers in their studies did not consider dimensional constraints or limitations related to overload resulting from the impact. No information was found describing how to manipulate the parameters of the frustum to achieve the desired values of energy absorption indicators (crashworthiness indicators). As filling for energy-absorbing elements, metallic foams (aluminum) were most commonly chosen. There was no research using polypropylene foam as a filling, especially for the prism frustums. There is also no confirmation regarding the behavior and correlation of the foam with the metal casing for different geometric parameters, e.g., prism frustums. This foam, unlike the foams used by the authors of the studies, is a closed-cell foam, which has a significant impact on its strength and behavior.

Apart from energy absorption during vehicle collisions, there is also a need to design structures capable of dissipating energy from pressure waves and explosions, which accompany us in various aspects of everyday life – from industrial processes to accidental or intentional detonations. Mazurkiewicz et al. [63] investigated the influence of blast loading on the load-carrying capacity of steel I-columns, highlighting the critical role of structural detailing under high-intensity pressure waves. Małachowski and co-authors proposed optimization strategies for protective panels in critical supporting elements, demonstrating how composite solutions can enhance energy dissipation and mitigate structural damage [64]. Further research has focused on vehicle chassis subjected to blast loading, providing insights into tire strength improvement and overall survivability under explosive threats [65]. These works emphasize the necessity of considering fluid-structure interaction and advanced energy absorption mechanisms when designing for extreme dynamic environments.

Thus, the motivation of the present research was to bridge a gap in the field of issues mentioned above, solving the problem of the energy absorption and optimization of frustum-shaped

prismatic columns, hollow and filled with polypropylene foam. The objectives of the work were: parametric study and the development of a simple optimization algorithm for a foam-filled thinwalled profile using FEM calculations. Such an algorithm would be useful in the preliminary design phase of the absorber.

Subject of the study

The subject of the research was a thin-walled prismatic truncated pyramid, both empty and foamfilled, with a square base (Figure 2a), made of two steel channel section columns connected using a lap joint with a series of spot welds. The details of the joining method are shown in Figure 2b.

The studied object is a truncated regular quadrilateral pyramid with a base edge length of a = 80 mm (Figure 2), height h, wall thickness t, and apex angle α. The material used in the theoretical parametric study was high-quality dual-phase steel DP800, with the following basic mechanical parameters: Young's modulus: 210 GPa, Poisson's ratio: 0.29, density: 7850 kg/m³, and yield strength: 590 MPa [66]. The distance between spot welds and the diameter of the weld were w = 20 mm and d = 4 mm, respectively. As a result, the number of spot welds is equal to 7. Metal plates with a thickness of 3 mm and relatively higher strength were welded to the upper and lower edges of the truncated section. The width of the overlap was 20 mm.

The material used to fill the frustum was EPP90 foam. It is a closed-cell foam with a density of 90 kg/m³. The main parameters of the filling material (EPP foam) were: Ef = 14.65 MPa, v = 0.03 [67]. The density of the foam was chosen as optimal from the perspective of energy absorption based on the stress-strain curve of EPP foam [68].

A parametric study of the hollow frustum was conducted based on three parameters: the height of the frustum h, the wall thickness t, and the angle of inclination α . The square base of the frustum had a constant dimension of a = 80 mm. The range of the studied parameters was as follows: h = {160; 200; 240 mm}, t = {0.8; 1; 1.6 mm}, and the angle of inclination α ranged from 0° to 10° with an increment of 1° . An exception was made for frustums with a height of h = 240 mm, where the maximum angle was 8° , due to geometric constraints with the fixed dimensions of the lower base of the frustum. This limitation meant that for larger angles, the shape was a regular pyramid. A total of 84 cases of

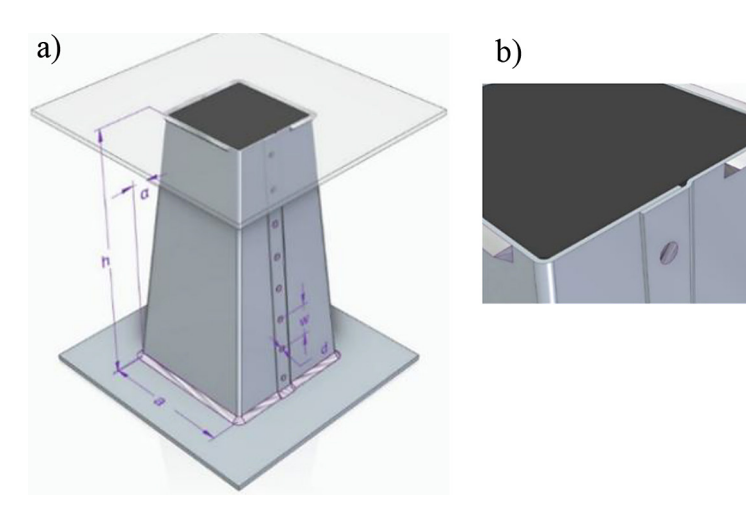


Figure 2. Thin-walled prismatic frustum: a) – general view, b) – spot weld joint

empty frustums were examined, the specifications of which are presented in Table 1.

In the parametric study of the frustum filled with foam, the range of the studied geometric parameters (h, t) remained the same, except for the truncated angle α , which varied from 0° to 10° (8° for h = 240 mm) in increments of 2°. In summary, 51 cases of the foam-filled frustum were examined, the specifications of which are presented in Table 2.

CRASHWORTHINESS PERFORMANCE ANALYSIS – CRASHWORTHINESS INDICATORS

There are several crashworthiness indicators [69–73] used to evaluate the crashworthiness performance and the energy absorption capacity of an absorber. A typical force – displacement curve for a thin-walled member subjected to axial impact is shown in Figure 3. In the present analysis the following indicators were used in the parametric study:

 PCF (peak crushing force) – the value of the crushing force achieved for the first peak on the force-displacement curve (Figure 3), F_{max} – maximum force in the range [0,d]. MCF (mean crushing force) – the average crushing force in the range [0,d] – the total absorbed energy divided by the distance of the crushed structure obtained from the forcedisplacement curve

$$MCF = \frac{EA(dx)}{d_x} [N]$$
 (1)

• EA (energy absorbed) – the energy absorbed is equal to the work done by the crushing force during the crushing process

$$EA(dx) = \int_0^{d_x} F(x)dx \ [J] \tag{2}$$

SEA (specific energy absorption) – the specific energy absorption is defined as the ratio of absorbed energy to the mass of the absorber.

$$SEA = \frac{EA}{m} \tag{3}$$

- CLE/CFE* (crush load efficiency/crush force efficiency) – it is a dimensionless indicator and is defined in two ways:
 - 1) First definition MCF to PCF ratio

Table 1. Geometric parameters of hollow frustums

h [mm]	t [mm]	α	Σ	
160	0.8, 1, 1.6	0°;1°;2°;3°;4°;5°;6°;7°;8°;9°;10°	30	
200	0.8, 1, 1.6	0°;1°;2°;3°;4°;5°;6°;7°;8°;9°;10°	30	
240	0.8, 1, 1.6	0°;1°;2°;3°;4°;5°;6°;7°;8°	24	
		Σ = 84		

h [mm]	t [mm] α		Σ		
160	0.8, 1, 1.6	0°;2°;4°;6°;8°;10°	18		
200	0.8, 1, 1.6	0°;2°;4°;6°;8°;10	18		
240*	08116	0.50.40.60.80	15		

Table 2. Geometric parameters of foam-filled frustums

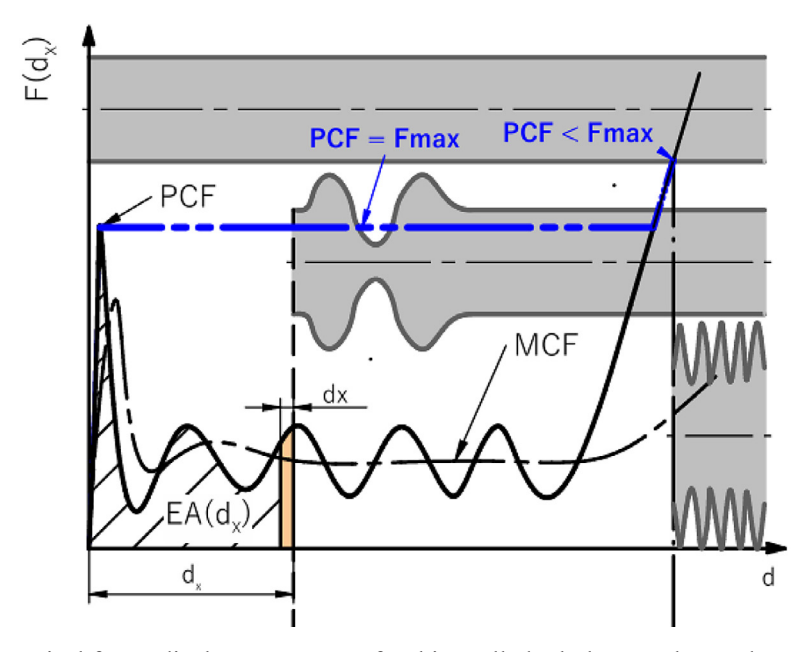


Figure 3. Typical force-displacement curve for thin-walled tubular member under axial impact

$$CLE = \frac{MCF}{PCF} \cdot 100 \, [\%] \tag{4}$$

2) Second definition – MCF to F_{max} ratio

$$CLE = \frac{MCF}{F_{max}} \cdot 100 \, [\%] \tag{5}$$

• TE (total efficiency) – the overall/total efficiency of the energy absorber. It is the maximum value of the ratio of energy absorbed to the product of the maximum force F_{max} and the length (height) of the energy absorber

$$TE = \frac{EA}{F_{max} \times l} \tag{6}$$

- d_{max} deformation, for which TE indicator is of maximum value.
- D_c (deformation capacity, relative deformation) the ability to deform, relative deformation. It is defined as the ratio of the shortening to initial length.

$$D_c = \frac{d}{l} \tag{7}$$

SE (stroke efficiency, effective crush distance)
non-dimensional d_{max} to initial length ratio.

$$SE = D_c(d_{max}) \tag{8}$$

METHODOLOGY

The flow chart in Figure 4 shows the methodology for optimizing the design using numerical analysis and artificial neural networks (ANN).

The process begins with a parametric study using the finite element method (FEM), the results of which serve as training data for artificial neural networks. The trained model is then used in the optimization process, leading to the identification of the most effective design solution. At the same time, experimental validation of the simulation results is carried out, as well as data analysis and visualization, which supports the interpretation of the results. The entire methodology is applied to a specific engineering problem, providing an example of the practical implementation of the described approach.

Finite element analysis

The FE model has been described in details in [74]. FE simulations were conducted using commercial ABAQUS® software. Figure 5a and 5b shows the shell model of the frustum used for the simulation. Frustum models were created using 4-node shell elements S4R (Figure 5c). The end edges of the frustum was attached to two rigid plates (R3D4) which were connected by tie links. The lower plate was fixed in space and on the second one the references point was created, where impactor mass and velocity was attached as well as shortening was recorded. Spot welds were modeled using fastener option [75]. The filling foam was modeled using solid elements C3D8R. Elastic-plastic material model with kinematic-isotropic hardening based on Cowper-Symond constitutive material model, describe by relation (9) was chosen for the simulations. Dynamic effects of strain rates are taken into account. Equivalent stress and equivalentn plastic strain were calculated using Huber-Mises yield criterion.

The analysis was conducted in two stages. In the first stage, an eigenvalue buckling analysis was performed to determine the critical buckling loads and corresponding mode shapes. These buckling modes were then used as initial geometric imperfections in the second stage, scaled to 10% of the wall thickness. The second stage involved a non-linear explicit dynamic

analysis, from which load-shortening curves were obtained.

$$\overline{\sigma_0} = \sigma_Y \left[1 + \left(\frac{\dot{\varepsilon}}{D}\right)^{1/q} \right] \tag{9}$$

where: $\overline{\sigma_0}$ is a current yield (proof) stress, $\sigma_{\rm Y}$ is the initial yield (proof) stress at static load, $\dot{\varepsilon}$ is the current strain-rate, and q and D are empirical coefficients of Cowper-Symonds relation.

Parameters D and q for DP 800 steel were taken from literature data [66] and confirmed by tensile test results performed by the authors [74]. In the analysis the following values were assumed: q = 4.79, D = 110105 for steel. The corresponding parameters for EPP foam were taken from literature [67] and were of following values q = 5, D = 3025 for foam.

Experimental validation of FEM simulations

In order to validate the FE model and simulations results the experimental tests were carried out using a drop hammer of the Instron CEAST 9350 HES (high-energy system) Drop Tower, whose overall view is shown in Figure 6a. An example of a frustum mounted in the device is shown in Figure 6b. The detailed description of experimental tests, their results and comparative analysis of FE versus

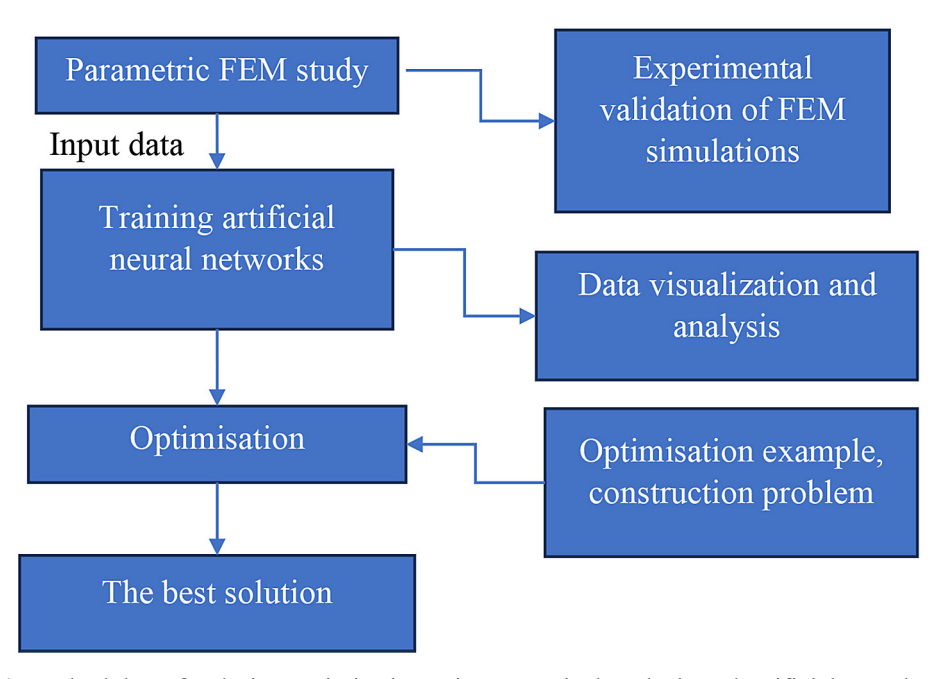


Figure 4. Methodology for design optimisation using numerical analysis and artificial neural networks.

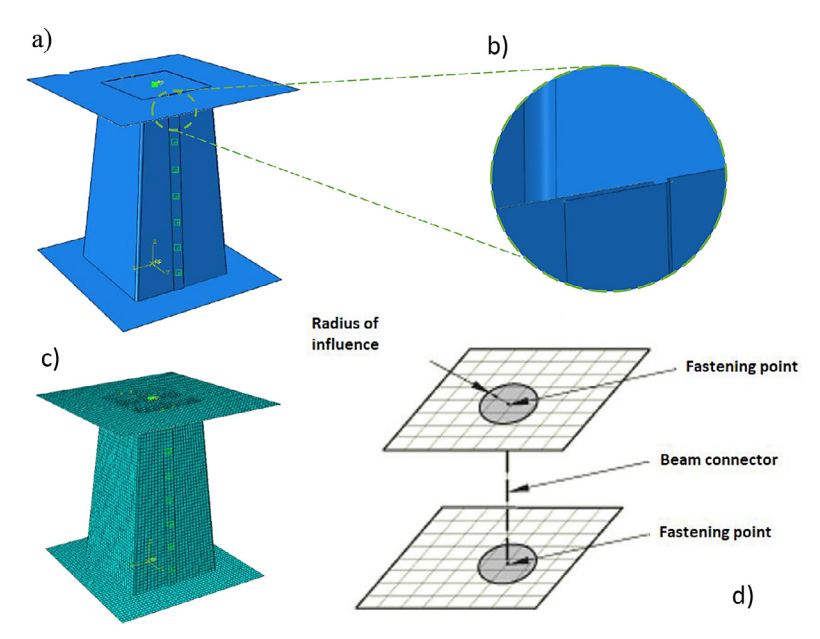


Figure 5. Finite element model: (a) shell model frustum, (b) place joining, (c) discrete model (d) fasteners model

experiment are presented by the authors in [76]. Exemplary load-shortening diagrams are shown in Figure 7.

Application of artificial neural networks (ANN) in the optimization procedure

In this paper, artificial neural networks were created using STATISTICA® software. The dataset obtained through numerical FE simulations served as the input data for training

the ANN. The input variables were the height of the absorber h, the wall thickness t, and the angle of inclination α . The output variables were the values of the indicators PCF, Fmax, EA, TE. In the learning process, the default learning parameters of the network were used. The purpose of this approach was to check whether satisfactory results could be obtained by leaving the default values, or if there is a need for a more detailed user awareness. The sampling method was random, i.e., cases were

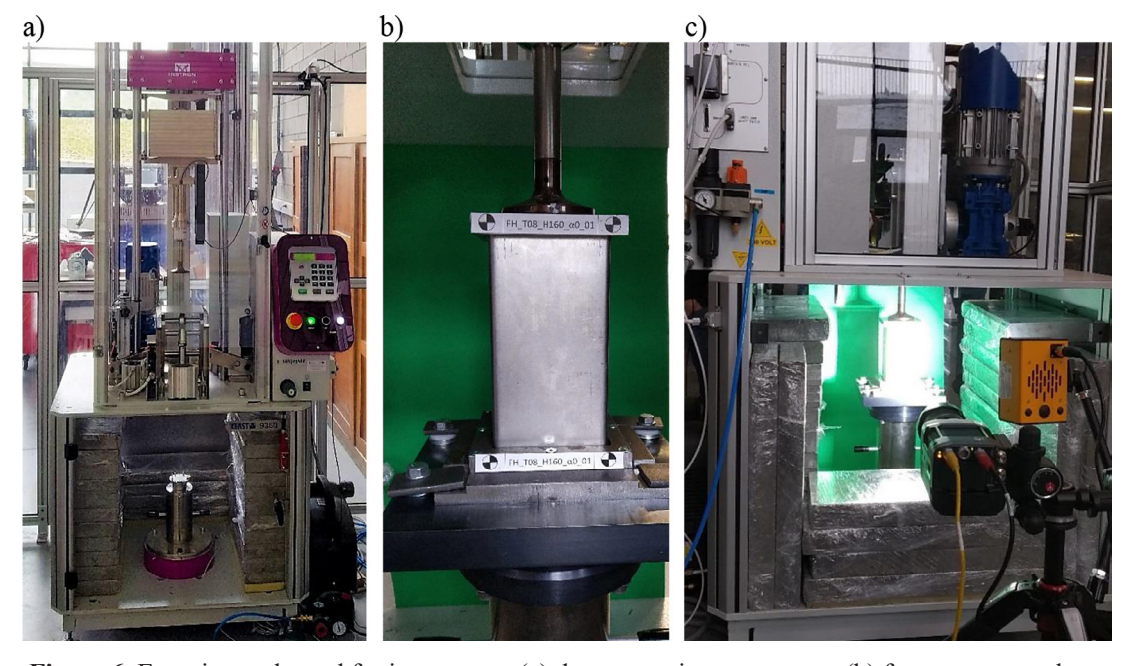


Figure 6. Experimental stand for impact test: (a) drop tower impact system, (b) frustum at test place, (c) high speed camera mounted on stand during experiment.

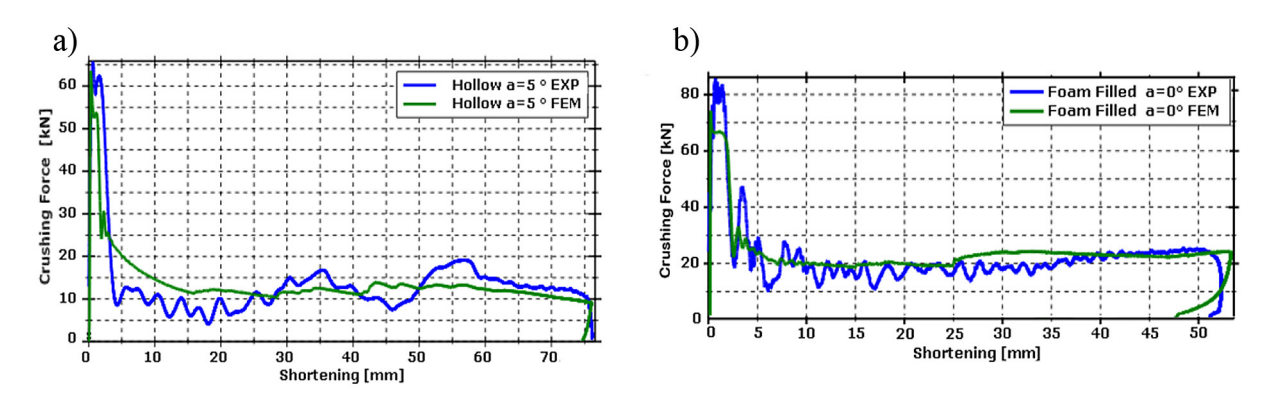


Figure 7. The exemplary comparative load-shortening diagrams (experiment vs. FEM): a) hollow frustum, inclination angle $\alpha = 5$, b) foam filled parallelepiped, inclination angle $\alpha = 0$.

drawn from the set of all input data cases for the training set, test set, and validation set. The sets contained the following percentages of input data: training -70%, test -15%, validation - 15%. An MLP perceptron was used, with the number of neurons in the hidden layer limited to a range of 3 to 150 neurons. A network of 100,000 was trained. From which 60 best ones in terms of learning quality were retained. The activation functions in the hidden and input neurons included: linear, logistic, hyperbolic tangent, and exponential functions. The error function used to assess the quality of the network was the sum of least squares. Tables 5 and 6 (Appendix) show the 20 best networks in terms of learning quality out of the retained 60. In the case of training the network for the empty frustum scenario, the learning quality was above 0.99, the testing quality above 0.97, and the validation above 0.98. On the other hand, the Neural Networks created for the data of the foam filled frustum achieved slightly poorer metrics: learning quality was practically at 0.97, testing quality ranged from 0.94 to 0.98, and validation quality ranged from 0.97 to 0.98. The lower quality metrics of the networks could have been influenced by a smaller number of training data caused by the long computation time. Despite the lower values of learning quality, they remain at a high level.

Thanks to the created ANNs, predictions for new, previously unstudied data were performed. For unfilled frustums, a MLP3-94-4 network was used, while for frustums filled with foam, a MLP3-102-4 network was utilized. Networks with the best performance in terms of learning quality were used.

MULTI-OBJECTIVE OPTIMIZATION

Optimization results

Figure 8, graphs for the energy absorption indicator EA are presented. Special attention should be paid to Figure 8b). It shows the dependence of EA on the parameters h and α . It is noticeable that for height values around h = 160 mm and α equal to 5°, the surfaces exhibit monotonicity changes. This change varies with the increase in height of the indicator EA and disappears with the increase in height. The indicator EA reaches a maximum at a wall thickness of t = 1 mm for the parameter values h and α from the previously defined set. In Figure 9, the obtained surface plots for the PCF and EA indicators for empty and filled frustums are presented. A comparison of the graphs in Figure 9a) and b) (without filling and with foam filling) shows that the previously described dependencies are weaker. The shape of the surface is also different. The observed energy values are greater for the frustum filled with foam. The same applies to the PCF indicator values (Figure 9c and 9d).

The most visible changes in the shape of the surface representing the values of the absorbed energy indicator EA are shown in the graphs placed in Figure 10a and 10b, while 10c and 10d compare the overall efficiency TE. Analyzing the graph in Figure 10c, the values of the TE indicator for a wall thickness of 0.8 mm can be observed to reach a maximum at about 200 mm height for low values of the inclination angle α , while for higher values of the inclination angle α and for small height values h, it remains practically constant and increases with height. In the case of filling (Figure 10d), the value of this indicator remains at a

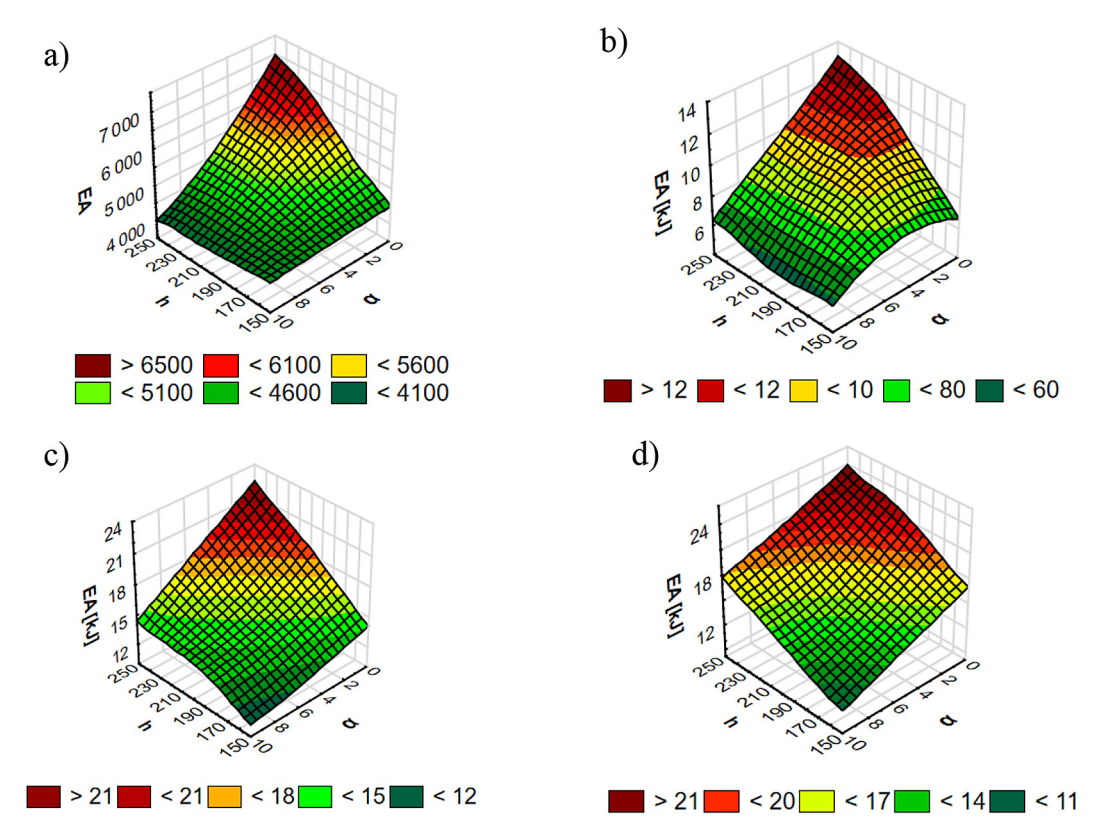


Figure 8. Surface plots representing the change in the EA indicator depending on the height h and the angle of inclination for an empty frustum for wall thicknesses: a) t = 0.6 mm, b) t = 1 mm, c) t = 1.4 mm d) t = 1.6 mm

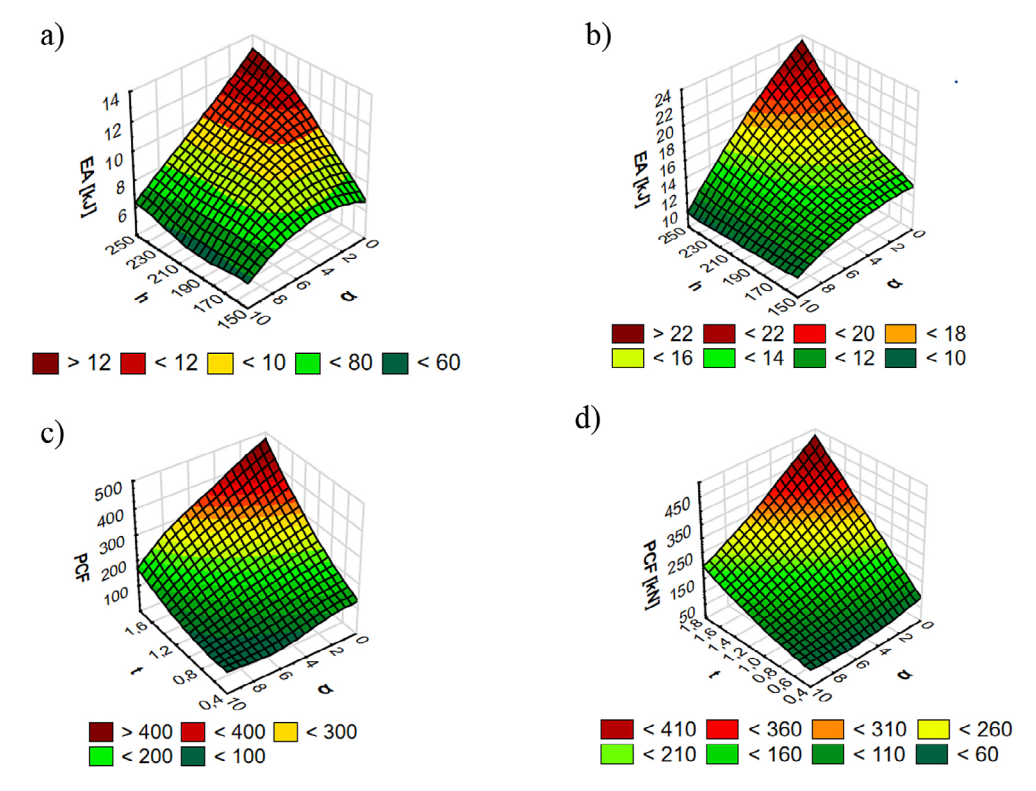


Figure 9. Comparison of surface graphs representing changes in PCF and EA indices for empty and foam-filled frustums; EA for t = 1 mm - a) without filling vs b) filled with foam; PCF for h = 220 mm - ac) without filling vs d) filled with foam.

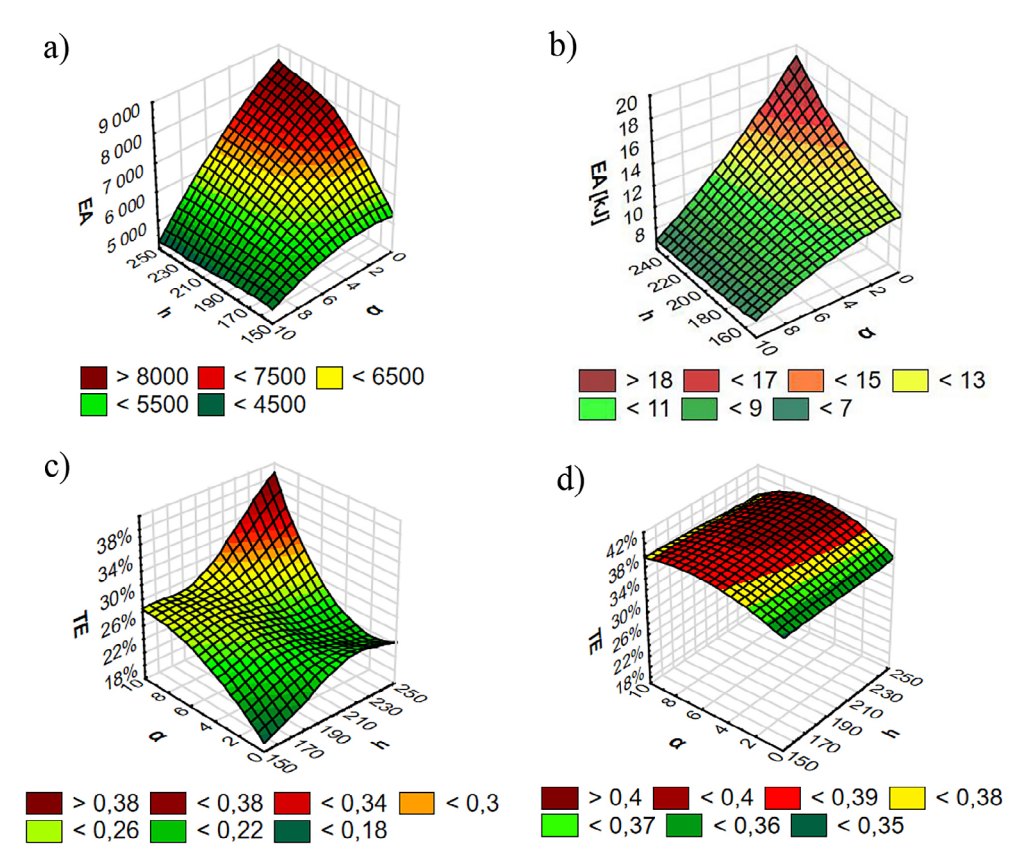


Figure 10. Comparison of surface graphs representing changes in EA and TE indices for empty and foam-filled frustums; EA for t = 0.8 mm - a) without filling vs b) filled with foam; TE for t = 1 mm - c) without filling vs d) filled with foam

constant level. Analyzing the grid lines, it was determined that the optimal inclination angle α is around 5° and increases slightly for higher frustum height values.

CASE STUDY – OPTIMIZATION OF THE VEHICLE FRONT FRAME LAYOUT

As a case study the vehicle (bus) front frame layout was chosen. It was assumed, that an impact energy amounts 55 kJ, which roughly corresponds to the impact of a rigidly constructed car with a mass of 1500 kg and a speed of 30 km/h. These data correspond to the requirements of Regulation No. 29 of the UN ECE. Figure 11a) shows the front wall frame (known as the outline), which is an integral part of the vehicle's skeleton and is located at its front. Inside the frame, there is a beam, in the subject literature referred to as firewall. Parallel to this beam, there is a curved beam. This beam defines the outline of the front of the vehicle, which is struck by the impactor.

FE model of the virtual test stand

Optimization calculations were also carried out using ABAQUS® [167] software. Shell elements (S4R) were used for the discretization of the front wall frame elements and the frustum. The wall thickness of the front frame profiles was set to 3 mm. For the filling foam, solid elements C3D8R were used as in the parametric study. The geometry of the FE virtual model is shown in Figure 12.

The impactor was modeled according to the requirements of Regulation No. 29 of the UN ECE, as a rectangular prism connected with two beams. It was given the characteristic of a rigid body (Rigid Body) with a reference point RP-2 corresponding to the center of gravity of the rectangular prism part of the impactor. This point was assigned an initial velocity of 5.8 m/s, which, along with the mass of the impactor of 3238 kg, allowed for an impact energy of 54.463 kJ. At this point, between the ends of the impactor beams, a reference point RP-3 was created, which, using a multi-point constraint (MPC), was coupled with the surfaces of the beam ends. The swing

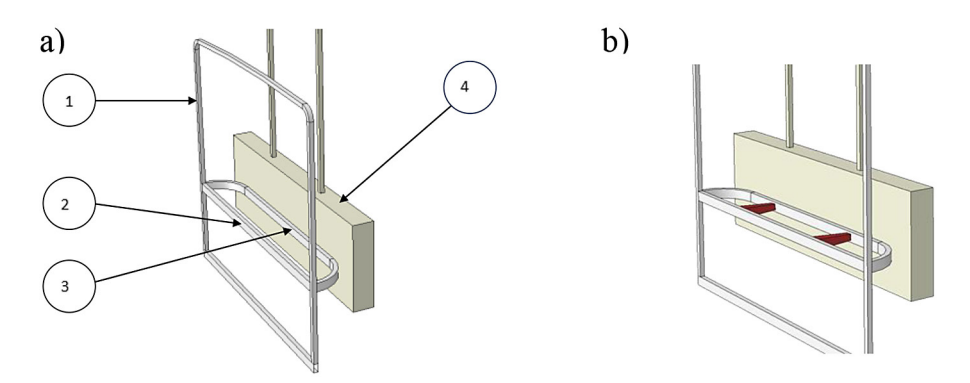


Figure 11. a) Front wall frame of the vehicle: 1 – outline; 2 – firewall; 3 – front outline curved beam; 4 – impactor, b) model of the front wall of the vehicle with the frustum geometry determined during optimization

of the pendulum (impactor) has been restricted by removing the appropriate degrees of freedom at the connected point RP-3. The results of FE simulations for the virtual stand without energy absorbing members are shown in Figure 13. The required impact energy was absorbed over a distance of 317 mm, measured for the point corresponding to the center of gravity of the impactor (Figure 13c).

Optimization of the energy absorbing members

In order to improve energy absorption, two energy-absorbing elements of the frustum type were placed between two parallel horizontal beams (Figure 11b). Another assumption is that each of them should be capable of absorbing energy of about 20 kJ. The height of the frustum is determined by the distance between the beams and is equal to h = 250 mm. The wall thickness t ranges from 0.8 to 2 mm. A significant limitation is the angle of inclination of the walls, which, for structural reasons, cannot be too large. The last significant limitation is the value of the PCF. It has been limited to the range of 80 kN to 300 kN. The minimum value from the range was imposed by the smallest value from the training data. The maximum value was determined according to biomechanical criteria.

STATISTICA® software was used for optimization of the hollow frusta. From the previously trained neural networks, 5 networks with the highest quality values were selected. The Simplex algorithm was used. As a result of the optimization, tables with predicted values of geometric parameters as well as the predicted value of the PCF strength were obtained (Table 3). For each of the networks, the optimal solution was found for

a wall thickness of about 1.46 mm. The first two networks defined the optimal angle in the vicinity of 3.75°. Meanwhile, the other three determined it at about 2.9° (Figure 14c). Similar convergences apply to the predicted value of the PCF. According to the majority principle, in the next stage, the forecasts from the three networks, that constituted the majority, were used.

For practical reasons, the obtained values were rounded to full dimensions. Based on the obtained data, the model was tested for established values of geometric parameters: t=1.5 mm, h=250 mm, $\alpha=3^{\circ}$. Images from the subsequent stages of the simulation are presented in Figure 16. It was possible to absorb energy over

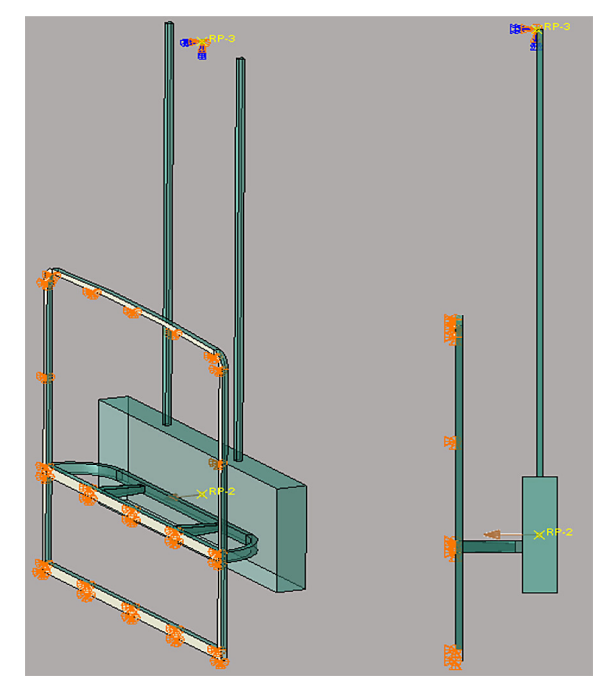


Figure 12. Geometry of the virtual test stand according to the Regulation No. 29 of the UN ECE

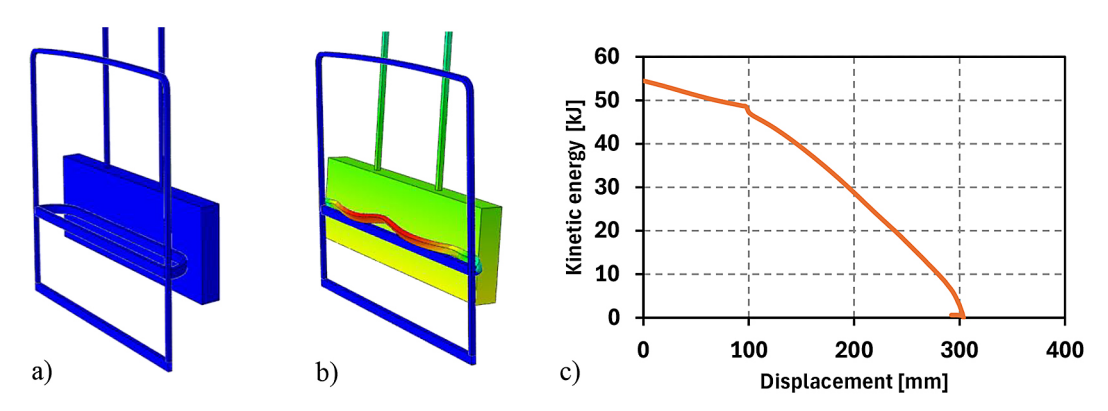


Figure 13. Results of the FE analysis of the impact on the front wall of the vehicle according to regulation No. 29 of the UN ECE. a) Initial state; b) Deformation of the front beam c) kinetic energy in terms of the impactor displacement

Table 3. Results of predicted parameter values by the ANN for the hollow frustum. The values used to develop the model are marked in red

SANNModel	PCF Independent	α Independent	h Independent	t Independent	EA Predicted
SANNModel	249514,1	3.745313	250	1.463747	20000,00
SANNModel	254172,5	3.877522	250	1.451744	20000,00
SANNModel	287142,0	2.900908	250	1.480735	20000,00
SANNModel	290117,2	2.982565	250	1.465594	20000,00
SANNModel	290887,6	2.958469	250	1.465108	20000,00

a shorter distance (230 mm), as schematically shown in Figure 15.

An analogous method was used to optimize the frustums filled with EPP90 foam. The results

obtained are presented in Table 4. The first four networks predicted an inclination angle α of approximately 4.3°, while the last fifth network predicted this angle to be close to 5°. The wall

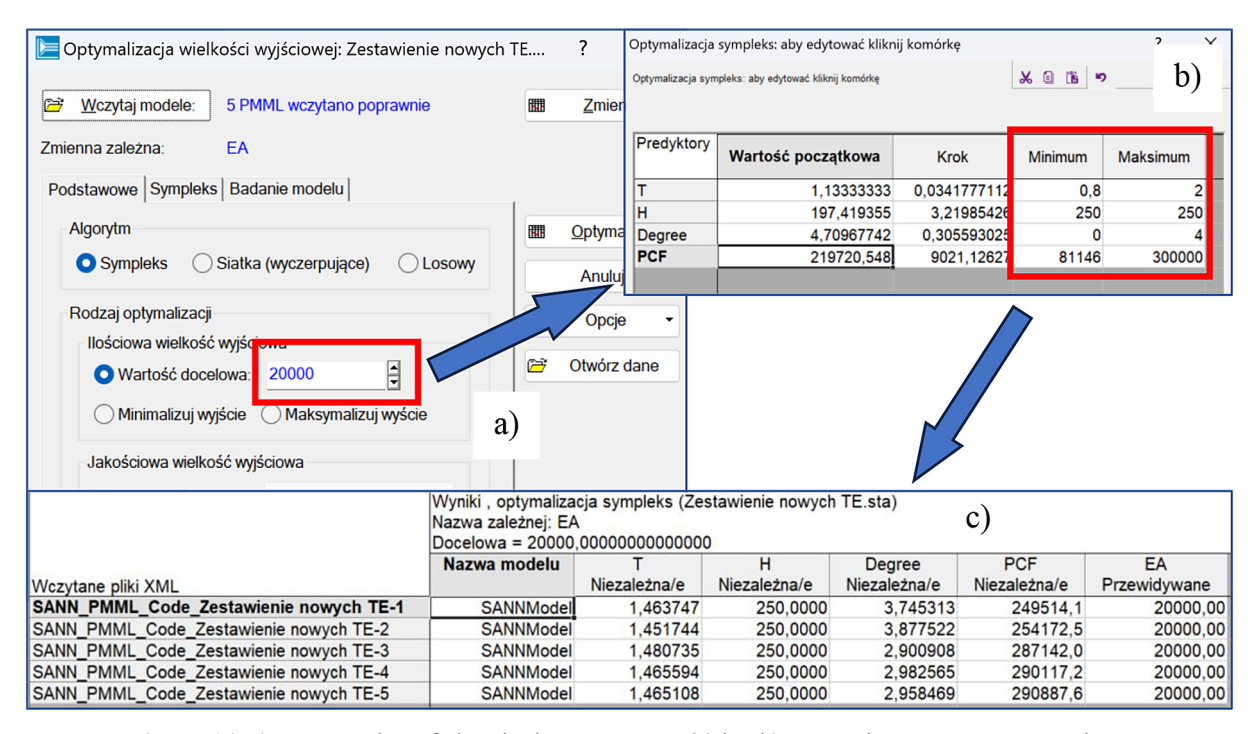


Figure 14. a) Target value of absorbed energy EA = 20 kJ; b) constraints on parameter values, c) optimization results

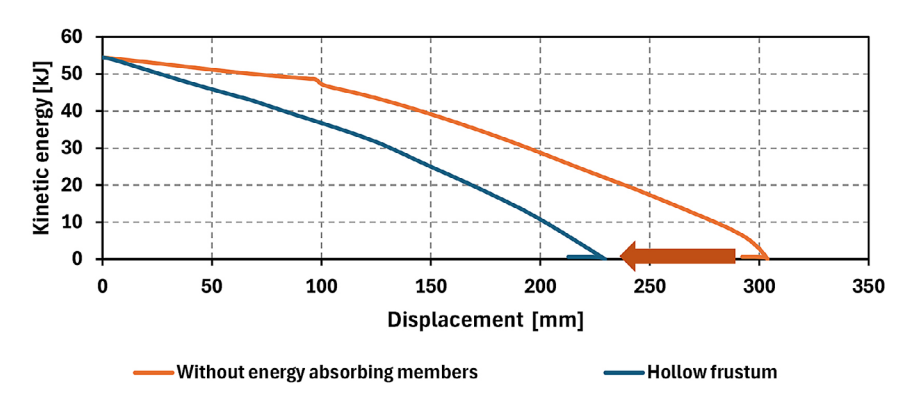


Figure 15. Kinetic energy in terms of the impactor displacement for the virtual stand without energy absorbing members and for the hollow frustum application

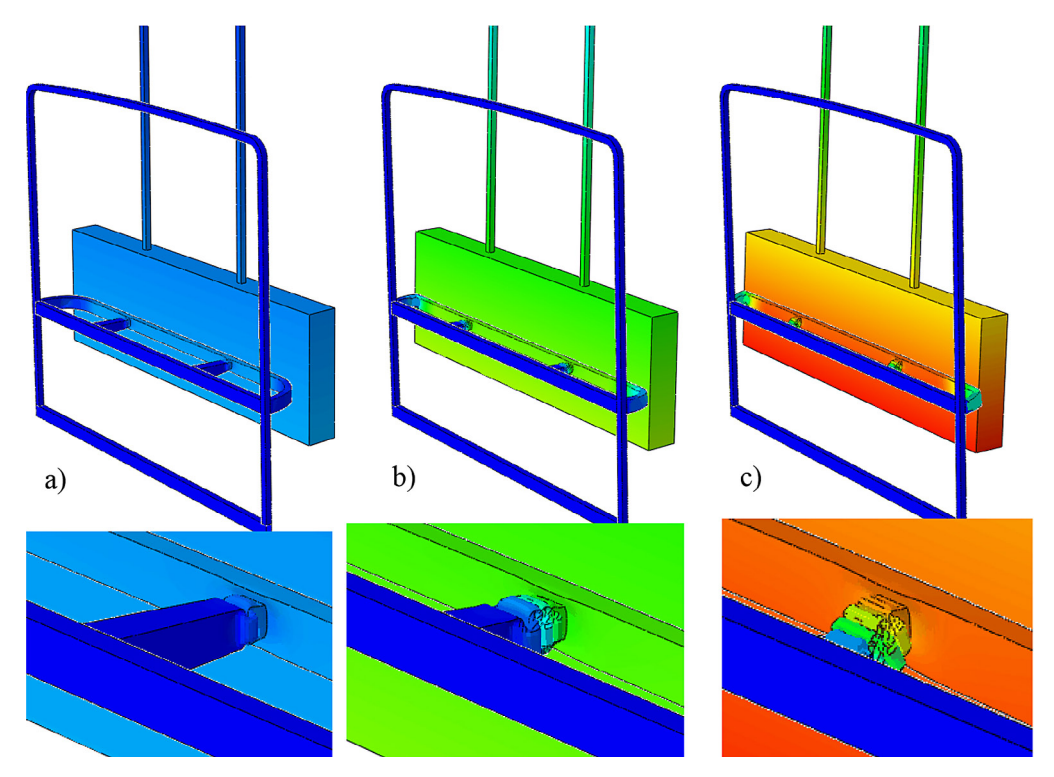


Figure 16. Subsequent deformation modes of the front wall frame of the vehicle, with energy absorbing members frustum type (hollow, FE simulation)

Table 4. Results of the predicted parameter values by the ANN for the foam-filled frustum. The values used to develop the model are marked in red

SANNModel	PCF Independent	α Independent	h Independent	t Independent	EA Predicted
SANNModel	206474,5	4.305185	250,0000	1.170562	20000,00
SANNModel	207188,4	4.321641	250,0000	1.172790	20000,00
SANNModel	207589,4	4.327139	250,0000	1.172936	20000,00
SANNModel	208624,1	4.337467	250,0000	1.173383	20000,00
SANNModel	219875,3	4.989882	250,0000	0.940937	20000,00

thickness is also similar for the first four, measuring t = 1.17 mm, as well as the values of the PCF force. Like in the case of the hollow frustums, the principle of majority was applied.

Based on the received data, the parameters were established: t = 1.2 mm, h = 250 mm, $\alpha = 4.5^{\circ}$. The deformation modes from the subsequent stages of the FE simulation are presented

in Figure 17. In this examined variant, the kinetic energy of the impactor was absorbed over a distance of about 250 mm. This value is smaller than in the basic case, i.e., without energy-absorbing elements, but larger than in the case of the frustum without filling. The considered case of the foam-filled frustum has a different geometry than the case of the frustum without filling. A comparison of the absorbed kinetic energy as a function of displacement has been presented for all cases examined so far in Figure 18.

The last case, additional, for which the FEM calculations were performed is the filling of a frustum with geometry as in the first optimization, namely: t = 1.5 mm, h = 250 mm, $\alpha = 3^{\circ}$.

This case is not covered by any software or criterion algorithm. In this case, the impact energy was absorbed over a distance of 220 mm (Figure 20). The foam filling, despite non-axial deformation in the later stage of the impact, reduced the distance over which energy is absorbed and stabilized the mode of deformation. Further deformation modes are presented in Figure 19.

FINAL REMARKS AND FURTHER RESEARCH PERSPECTIVES

In the paper the multi-objective optimization of thin-walled frustum-type structures (truncated

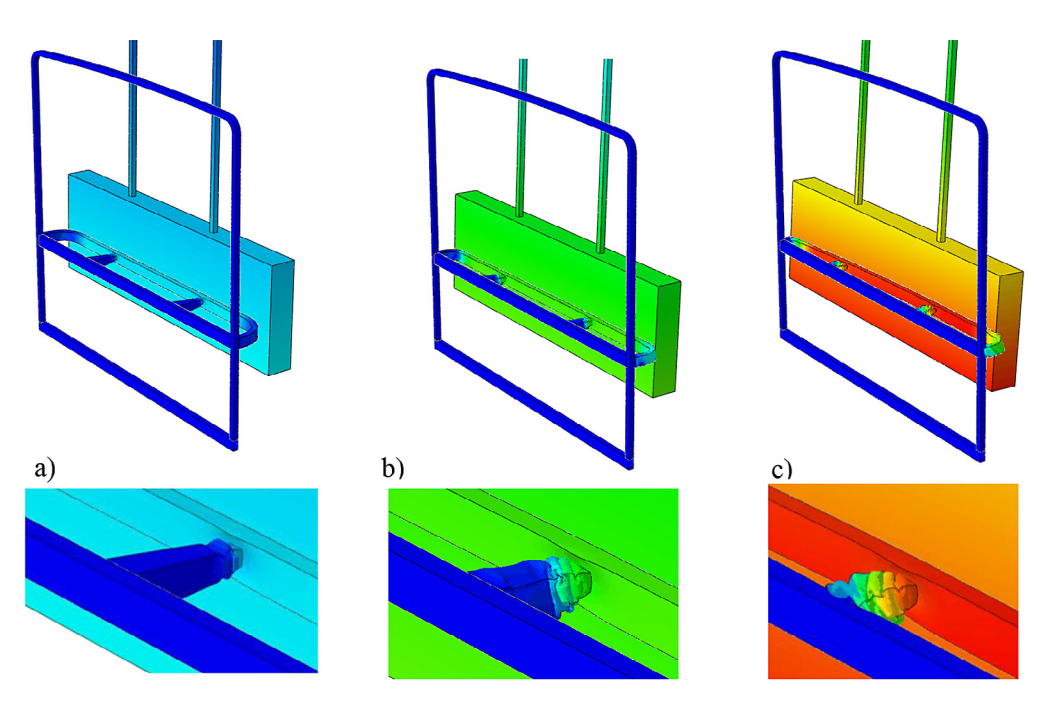


Figure 17. Subsequent deformation modes of the front wall frame of the vehicle, with energy absorbing members frustum type (foam filled, FE simulation)

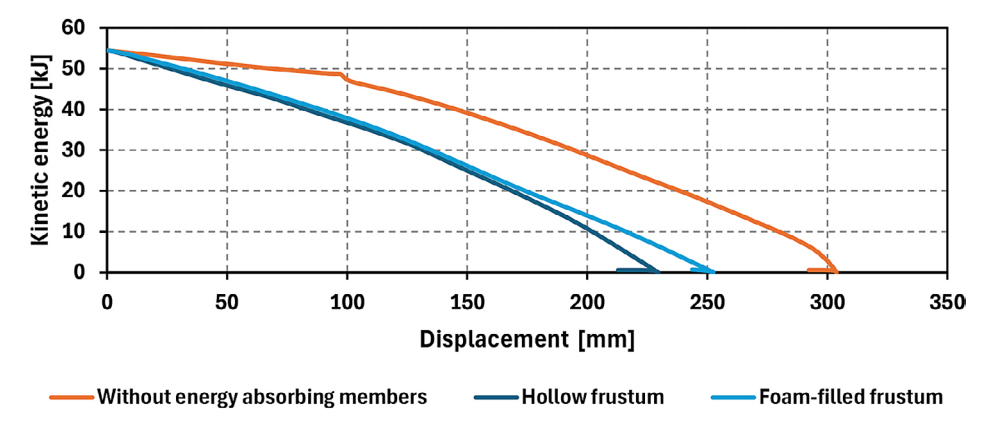


Figure 18. Kinetic energy in terms of the impactor displacement for the virtual stand without energy absorbing members and for the hollow frustum application and with foam-filled frustums applied

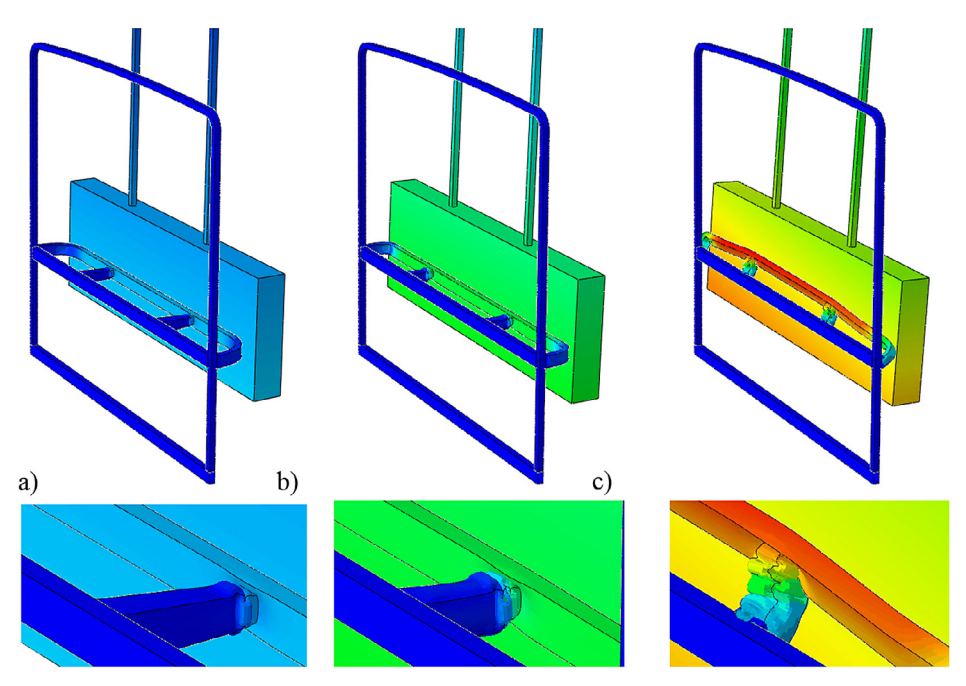


Figure 19. Subsequent deformation modes of the front wall frame of the vehicle, with energy absorbing members frustum type (foam filled, FE simulation) with the following parameters: T = 1.5 mm, H = 250 mm, $\alpha = 3^{\circ}$

pyramids) made of steel, both empty and filled with EPP foam is presented. The research involved an extensive FEM-based parametric study in the ABAQUS® environment, covering over 130 geometric variants of frustum structures, validated by the experimental tests. Experimental studies confirmed the usefulness of the developed numerical FEM model for conducting multi-objective parametric analyses and optimization. An optimization algorithm based on ANN was developed, enabling rapid prediction of optimal structural parameters for given energy absorption requirements. The algorithm was tested on a vehicle homologation structure, demonstrating its

effectiveness in selecting a geometry that ensures the absorption of a specified amount of energy while maintaining dimensional constraints.

Increasing the angle α causes a decrease in the PCF indicator for both empty and filled frustums. The filling leads to an increase in PCF compared to the empty frustum regardless of the angle α . For empty frustums, increasing the angle α from 0° to 5° results in an increase in compressive strength efficiency (CLE) by 40 and 17.5% for experimental data and FEM simulation, respectively. However, for filled frustums, increasing the angle α from 0° to 5° results in a decrease in CLE by 29% (experiment) and 27% (FEM).

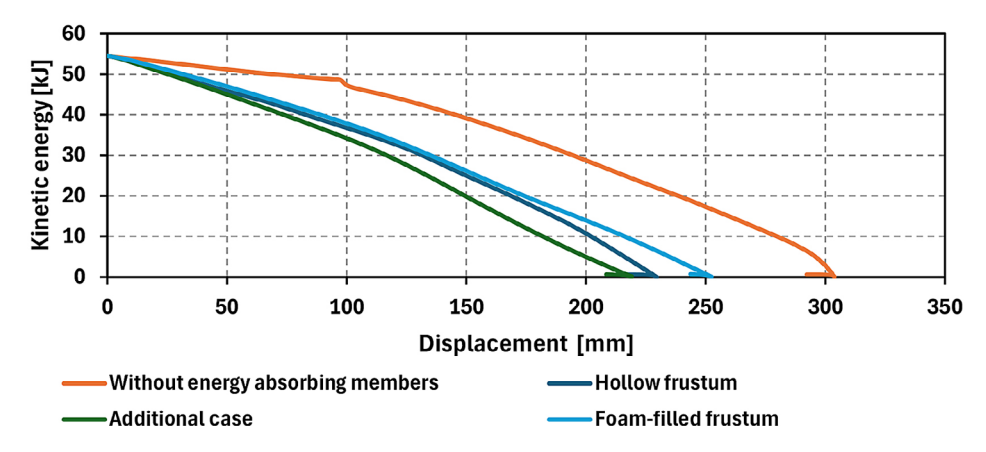


Figure 20. Kinetic energy in terms of the impactor displacement for the virtual stand without energy absorbing members and for the hollow frustum application, with foam-filled frustums applied and additional case

Filling a rectangular prism with foam ($\alpha = 0^{\circ}$) results in an increase of CLE by about 90% (both in the experiment and in the FEA simulation), while filling a frustum with foam ($\alpha = 5^{\circ}$) leads to a decrease in CLE by 4.5% (experiment) and an increase of 19% (FEA). In the case of empty frustums, increasing the angle α from 0° to 5° results in a 4.2% increase in total efficiency (TE). However, for filled frustums, increasing the angle α from 0° to 5° causes an increase in TE by 11.3% (FEM) and 13.3% (experiment).

As analyses of surface plots have shown, finding an optimally designed solution is complicated and time-consuming. Additionally, extremes may not exist at all, as in the case of absorbed energy EA. An optimally designed solution typically has more than one optimization criterion.

CONCLUSIONS

Based on the research conducted, the following conclusions can be drawn, which may indicate further directions for research:

- 1. The use of additional elements resulted in the beam not being located behind the firewall area. Using a smaller angle in the case of foam is not a desirable solution because it leads to bending earlier.
- 2. For the assumed energy absorption requirement EA = 20 kJ, the ANN for the variants of frustums filled with foam was designed with a larger wall inclination angle than for the unfilled variant, while having a thinner wall, which allowed reducing the PCF value by almost 30%.
- 3. The training dataset generated through parametric analysis based on the one-factor-at-atime (OFAT) method may exhibit limited representativeness and suboptimal efficiency for training artificial neural networks. Alternative approaches, such as random sampling of the parameter space or the application of design of experiments (DoE) methodologies, enable the construction of more diverse and informative datasets. This increased variability would enhance the generalization capability of neural networks and improve predictive accuracy across a broader range of input conditions. Furthermore, the use of DoE strategies may contribute to a reduction in the number of required training samples, thereby improving computational efficiency and lowering the overall cost of model development.

- 4. The optimization example presented here considers only one impact case. It is possible to consider multi-criteria optimization involving more than one case, which can lead to more comprehensive and accurate results. This approach will make the results more useful and functional
- 5. Case 4 shows that despite advances in computer technology, including artificial intelligence, the final decision in the optimization process is often best made by humans, thanks to their intuition and experience. However, well-used tools such as AI can greatly help in achieving the goal and speed up the entire process.
- 6. It is possible to extend this optimization to multi-component energy absorption systems. The key will be to collect sufficient data. In addition, the optimization must take into account the fact that the optimized modules must fit together. In this case, hierarchical optimization seems to be the best approach.
- 7. Extending the presented optimization approach by applying real-time feedback loops can improve the usability of this method. This may be particularly important for engineers working on crashworthiness.

REFERENCES

- Major Z, Bodnár L, Merczel DB, Szép J, Lublóy É. Analysis of the heating of steel structures during fire load. Emerg Sci J. 2024;8(1):1–16.
- Alghamdi AA. Collapsible impact energy absorbers: an overview. Thin-Walled Struct [Internet]. 2001 Feb;39(2):189–213. Available from: https://linkinghub.elsevier.com/retrieve/pii/S0263823100000483
- 3. Hammar I, Djermane M, Amieur B. Dynamic buckling analysis of ductile damage evolution for thin shell with Lemaitre's Model. Civ Eng J. 2024;10(3):835–46.
- Tang T, Zhang W, Yin H, Wang H. Crushing analysis of thin-walled beams with various section geometries under lateral impact. Thin-Walled Struct [Internet]. 2016;102:43–57. Available from: http://dx.doi.org/10.1016/j.tws.2016.01.017
- Sun G, Tian X, Fang J, Xu F, Li G, Huang X. Dynamical bending analysis and optimization design for functionally graded thickness (FGT) tube. Int J Impact Eng [Internet]. 2015;78:128– 37. Available from: http://dx.doi.org/10.1016/j. ijimpeng.2014.12.007
- Gibson LJ. Cellular Solids. MRS Bull [Internet]. 2003 Apr;28(4):270–4. Available from: http://link.

- springer.com/10.1557/mrs2003.79
- Bouix R, Viot P, Lataillade JL. Polypropylene foam behaviour under dynamic loadings: Strain rate, density and microstructure effects. Int J Impact Eng. 2009;36(2):329–42.
- 8. Zarei HR, Kröger M. Optimization of the foamfilled aluminum tubes for crush box application. Thin-Walled Struct. 2008;46(2):214–21.
- Alshannaq A, Tamimi M, Abu Qamar M. Sensitivity and optimization analysis of torsional behavior in multicellular thin-walled tubes. Civ Eng J. 2024 Sep 1;10:2902–18.
- 10. Asanjarani A, Mahdian A, Dibajian SH. Comparative analysis of energy absorption behavior of tapered and grooved thin-walled tubes with the various geometry of the cross section. Mech Adv Mater Struct [Internet]. 2020 Apr 15;27(8):633–44. Available from: https://doi.org/10.1080/15376494. 2018.1488311
- 11. Nia AA, Hamedani JH. Comparative analysis of energy absorption and deformations of thin walled tubes with various section geometries. Thin-Walled Struct. 2010 Dec 1;48(12):946–54.
- 12. Ramsey H. Plastic buckling of conical shells under axial compression. Int J Mech Sci. 1977 Jan 1;19(5):257–72.
- 13. Mamalis AG, Johnson W, Viegelahn GL. The crumpling of steel thin-walled tubes and frusta under axial compression at elevated strainrates: Some experimental results. Int J Mech Sci. 1984;26(11–12):537–47.
- 14. Aljawi AAN, Alghamdi AAA, Abu-Mansour TMN, Akyurt M. Inward inversion of capped-end frusta as impact energy absorbers. Thin-Walled Struct. 2005 Apr 1;43(4):647–64.
- 15. Mamalis AG, Manolakos DE, Ioannidis MB, Kostazos PK. Numerical simulation of thin-walled metallic circular frusta subjected to axial loading. International Journal of Crashworthiness. 2005;10:505–13.
- 16. Gupta NK, Sheriff NM, Velmurugan R. A study on buckling of thin conical frusta under axial loads. Thin-Walled Struct. 2006 Sep 1;44(9):986–96.
- 17. Gupta NK, Venkatesh. Experimental and numerical studies of impact axial compression of thin-walled conical shells. Int J Impact Eng. 2007 Apr 1;34(4):708–20.
- 18. Gupta NK, Mohamed Sheriff N, Velmurugan R. Analysis of collapse behaviour of combined geometry metallic shells under axial impact. Int J Impact Eng. 2008 Aug 1;35(8):731–41.
- 19. Mohamed Sheriff N, Gupta NK, Velmurugan R, Shanmugapriyan N. Optimization of thin conical frusta for impact energy absorption. Thin-Walled Struct. 2008 Jun 1;46(6):653–66.
- 20. Gupta PK. A study on mode of collapse of varying

- wall thickness metallic frusta subjected to axial compression. Thin-Walled Struct. 2008 May 1;46(5):561–71.
- 21. Ahmad Z, Thambiratnam DP, Tan ACC. Dynamic energy absorption characteristics of foam-filled conical tubes under oblique impact loading. Int J Impact Eng. 2010 May 1;37(5):475–88.
- Acar E, Guler MA, Gereker B, Cerit ME, Bayram B. Multi-objective crashworthiness optimization of tapered thin-walled tubes with axisymmetric indentations. Thin-Walled Struct. 2011 Jan 1;49(1):94–105.
- 23. Ghamarian A, Zarei HR, Abadi MT. Experimental and numerical crashworthiness investigation of empty and foam-filled end-capped conical tubes. Thin-Walled Struct. 2011 Oct 1;49(10):1312–9.
- 24. Gupta NK, Prasad GLE, Gupta SK. Plastic collapse of metallic conical frusta of large semi-apical angles. Vol. 2, International Journal of Crashworthiness. 1997;349–66.
- 25. Ghamarian A, Zarei H. Crashworthiness investigation of conical and cylindrical end-capped tubes under quasi-static crash loading. Int J Crashworthiness [Internet]. 2012 Feb 1;17(1):19–28. Available from: https://doi.org/10.1080/13588265.2011.623025
- 26. Zhang X, Zhang H. Relative merits of conical tubes with graded thickness subjected to oblique impact loads. Int J Mech Sci. 2015 Jul 1;98:111–25.
- Zhang X, Zhang H, Wen Z. Axial crushing of tapered circular tubes with graded thickness. Int J Mech Sci. 2015 Mar 1;92:12–23.
- 28. Zhang H, Zhang X. Crashworthiness performance of conical tubes with nonlinear thickness distribution. Thin-Walled Struct. 2016 Feb 1;99:35–44.
- Elahi SM, Rouzegar J, Assaee H. Axial splitting of conical frusta: Experimental and numerical study and crashworthiness optimization. Thin-Walled Struct [Internet]. 2018;127(February):604–16. Available from: https://doi.org/10.1016/j.tws.2018.03.005
- 30. Yang F, Wang M, Hassan MTZ, Meguid SA, Hamouda AMS. Effect of interfacial friction and fold penetration on the progressive collapse of foamfilled frustum using kinematically admissible model. Vol. 23, International Journal of Crashworthiness. 2018;581–92.
- 31. Elahi SM, Rouzegar J, Assaee H. Axial splitting of conical frusta: Experimental and numerical study and crashworthiness optimization. Thin-Walled Struct. 2018 Jun 1;127:604–16.
- 32. Shiravand A, Asgari M. Hybrid metal-composite conical tubes for energy absorption; theoretical development and numerical simulation. Thin-Walled Struct. 2019 Dec 1;145:106442.
- 33. Chahardoli S, Nia AA, Asadi M. Parametric investigation of the mechanical behavior of expanding-folding absorbers and their implementation in

- sandwich panels core. Thin-Walled Struct. 2019 Apr 1;137:53–66.
- 34. Patel V, Tiwari G, Dumpala R. Crashworthiness analysis of multi-configuration thin walled co-axial frusta tube structures under quasi-static loading. Thin-Walled Struct. 2020 Sep 1;154:106872.
- 35. El-Sobky H, Singace AA. An experiment on elastically compressed frusta. Thin-Walled Struct. 1999 Apr 1;33(4):231–44.
- 36. Kathiresan M. Influence of shape, size and location of cutouts on crashworthiness performance of aluminium conical frusta under quasi-static axial compression. Thin-Walled Struct. 2020 Sep 1;154:106793.
- 37. Feli S, Makhsousse E, Jafari SS. Dynamic progressive buckling of thin-wall grooved conical tubes under impact loading. Int J Crashworthiness [Internet]. 2020 Mar 3;25(2):220–9. Available from: https://doi.org/10.1080/13588265.2019.1573476
- 38. Kathiresan M. Influence of shape, size and location of cutouts on crashworthiness performance of aluminium conical frusta under quasi-static axial compression. Thin-Walled Struct. 2020 Sep 1;154:106793.
- Kathiresan M. Effects of cutout and impact loading condition on crashworthiness characteristics of conical frusta. Vol. 27, International Journal of Crashworthiness. 2022;1046–66.
- 40. Akhavan Attar A, Kazemi M. Novel geometric arrangement effects on energy absorption of a conical structure with various cross-sections. Thin-Walled Struct. 2022 Apr 1;173:109005.
- 41. Tuzgel F, Akbulut EF, Guzel E, Yucesoy A, Sahin S, Tasdemirci A, et al. Testing and modeling blast loading of a sandwich structure cored with a bioinspired (balanus) core. Thin-Walled Struct. 2022 Jun 1;175:109185.
- 42. Chen X, wang wenhao, Jin F, Fan H. Braided-textile reinforced thin-walled conical tubular structures: Designing, manufacturing and testing. Thin-Walled Struct. 2022 May 1;174:109121.
- 43. Kathiresan M. Effects of cutout and impact loading condition on crashworthiness characteristics of conical frusta. Int J Crashworthiness [Internet]. 2022;27(4):1046–66. Available from: https://doi.org/10.1080/13588265.2021.1903280
- 44. El-Sobky H, Singace AA, Petsios M. Mode of collapse and energy absorption characteristics of constrained frusta under axial impact loading. Int J Mech Sci. 2001;43(3):743–57.
- 45. Singace AA, El-Sobky H, Petsios M. Influence of end constraints on the collapse of axially impacted frusta. Thin-Walled Struct. 2001 May 1;39(5):415–28.
- 46. El-Sobky H, Singace AA, Petsios M. Mode of

- collapse and energy absorption characteristics of constrained frusta under axial impact loading. Int J Mech Sci. 2001 Dec 1;43(3):743–57.
- 47. Alghamdi AAA. Reinversion of aluminium frustra. Thin-Walled Struct. 2002 Dec 1;40(12):1037–49.
- 48. Alghamdi AAA. Folding-crumpling of thin-walled aluminium frusta. Int J Crashworthiness [Internet]. 2002 Jan 1;7(1):67–78. Available from: https://doi.org/10.1533/cras.2002.0207
- 49. Easwara Prasad GL, Gupta NK. An experimental study of deformation modes of domes and large-angled frusta at different rates of compression. Int J Impact Eng. 2005 Dec 1;32(1–4):400–15.
- 50. Reid SR, Reddy TY. Static and dynamic crushing of tapered sheet metal tubes of rectangular cross-section. Int J Mech Sci. 1986;28(9):623–37.
- 51. Mamalis AG, Manolakos DE, Viegelahn GL. The axial crushing of thin PVC tubes and frusta of square cross-section. Int J Impact Eng [Internet]. 1989 Jan 1 [cited 2025 Jan 6];8(3):241–64. Available from: https://linkinghub.elsevier.com/retrieve/pii/0734743X89900055
- 52. Mamalis AG, Manolakos DE, Demosthenous GA, Ioannidis MB. Energy absorption capability of fibreglass composite square frusta subjected to static and dynamic axial collapse. Thin-Walled Struct. 1996 Aug 1;25(4):269–95.
- 53. Mamalis AG, Manolakos DE, Ioannidis MB, Kostazos PK, Hassiotis G. Finite element simulation of the axial collapse of thin-wall square frusta. Int J Crashworthiness [Internet]. 2001 Jan 1;6(2):155–64. Available from: https://doi.org/10.1533/cras.2001.0169
- 54. Nagel GM, Thambiratnam DP. Dynamic simulation and energy absorption of tapered tubes under impact loading. Int J Crashworthiness. 2004;9(4):389–99.
- 55. Nagel GM, Thambiratnam DP. A numerical study on the impact response and energy absorption of tapered thin-walled tubes. Int J Mech Sci. 2004 Feb 1;46(2):201–16.
- 56. Nagel GM, Thambiratnam DP. Computer simulation and energy absorption of tapered thin-walled rectangular tubes. Thin-Walled Struct. 2005 Aug 1;43(8):1225–42.
- 57. Liu Y. Design optimisation of tapered thin-walled square tubes. Int J Crashworthiness [Internet]. 2008 Sep 11;13(5):543–50. Available from: https://doi.org/10.1080/13588260802222102
- 58. Qi C, Yang S, Dong F. Crushing analysis and multiobjective crashworthiness optimization of tapered square tubes under oblique impact loading. Thin-Walled Struct. 2012 Oct 1;59:103–19.
- Asanjarani A, Dibajian SH, Mahdian A. Multi-objective crashworthiness optimization of tapered thinwalled square tubes with indentations. Thin-Walled

- Struct [Internet]. 2017;116(July 2016):26–36. Available from: http://dx.doi.org/10.1016/j. tws.2017.03.015
- 60. Gan N, Yao S, Dong H, Xiong Y, Liu D, Pu D. Energy absorption characteristics of multi-frusta configurations under axial impact loading. Thin-Walled Struct. 2018 Jan 1;122:147–57.
- 61. Altin M, Kılınçkaya Ü, Acar E, Güler MA. Investigation of combined effects of cross section, taper angle and cell structure on crashworthiness of multicell thin-walled tubes. Int J Crashworthiness [Internet]. 2019 Mar 4;24(2):121–36. Available from: https://doi.org/10.1080/13588265.2017.1410338
- 62. Hong W, Lai C, Fan H. Frusta structure designing to improve quasi-static axial crushing performances of triangular tubes. Vol. 16, International Journal of Steel Structures. 2016. p. 257–66.
- 63. Mazurkiewicz Ł, Malachowski J, Baranowski P. Blast loading influence on load carrying capacity of I-column. Eng Struct. 2015 Dec 1;104:107–15.
- 64. Mazurkiewicz Ł, Małachowski J, Baranowski P. Optimization of protective panel for critical supporting elements. Compos Struct [Internet]. 2015;134:493–505. Available from: https://www.sciencedirect.com/science/article/pii/S026382231500762X
- 65. Baranowski P, Malachowski J. Numerical study of selected military vehicle chassis subjected to blast loading in terms of tire strength improving. Bull Polish Acad Sci Tech Sci. 2015 Dec 12;63:867–78.
- 66. Kaczyński P, Rusiński E. Ocena wytrzymałości połączeń w cienkościennych strukturach energochłonnych. Politechnika Wrocławska, 2014.
- 67. Kotełko M, Mołdawa A. Dynamic response of foam filled thin-walled frusta under axial impact. In: 7th International Conference on Coupled Instabilities in Metal Structures (CIMS), Baltimore, MD, 2016.
- 68. General Technical Information Neopolen [Internet]. 2016;1–10. Available from: https://documents.basf.

- com/1bc67bd6d3898c25bb6f6a75d60e63d884c34f 4f?response-content-disposition=inline
- 69. Zhang X, Cheng G, Zhang H. Numerical investigations on a new type of energy-absorbing structure based on free inversion of tubes. Int J Mech Sci. 2009;51(1):64–76.
- 70. Hanssen AG, Langseth M, Hopperstad OS. Static and dynamic crushing of circular aluminum extrusions with aluminum foam filler. Int J Impact Eng. 2000 May 1;24(5):475–507.
- 71. Hanssen AG, Langseth M, Hopperstad OS. Static and dynamic crushing of square aluminum extrusions with aluminum foam filler. Int J Impact Eng. 2000;24(4):347–83.
- 72. Kotełko M, Ferdynus M, Jankowski J. Energy absorbing effectiveness Different approaches. Acta Mech Autom. 2018;12(1):54–9.
- 73. Jones N. Energy-absorbing effectiveness factor. Int J Impact Eng. 2010 Jun 1;37(6):754–65.
- 74. Szklarek K, Kotełko M, Ferdynus M. Crashworthiness performance of thin-walled hollow and foamfilled prismatic frusta FEM parametric studies Part 1. Thin-Walled Struct [Internet]. 2022 Dec 1 [cited 2025 Aug 6];181:110046. Available from: https://www.sciencedirect.com/science/article/abs/pii/S0263823122006206
- Reddy S, Abbasi M, Fard M. Multi-cornered thin-walled sheet metal members for enhanced crashworthiness and occupant protection. Thin-Walled Struct [Internet]. 2015;94:56–66. Available from: http://dx.doi.org/10.1016/j.tws.2015.03.029
- 76. Ferdynus M, Szklarek K, Kotełko M. Crashworthiness performance of thin-walled hollow and foamfilled prismatic frusta, Part 2: Experimental study. Thin-Walled Struct [Internet]. 2022 Dec 1 [cited 2025 Aug 6];181:110070. Available from: https://www.sciencedirect.com/science/article/abs/pii/S026382312200636X?via%3Dihub